Check for updates

Received: 18 February 2021 | Revised: 8 November 2021 | Accepted: 5 December 2021

DOI: 10.1002/aic.17586

AIChE JOURNAL

RESEARCH ARTICLE

Process Systems Engineering

Design of shell and tube heat exchangers considering the interaction of fouling and hydraulics

Julia C. Lemos[1] | André L. H. Costa[1] | Miguel J. Bagajewicz[2]

[1]Institute of Chemistry, Rio de Janeiro State University (UERJ) Rua São Francisco Xavier, Rio de Janeiro, Brazil

[2]School of Chemical, Biological and Materials Engineering, University of Oklahoma, Norman, Oklahoma, USA

Correspondence
André L. H. Costa, Institute of Chemistry, Rio de Janeiro State University (UERJ), Rua São Francisco Xavier, 524, Maracanã, Rio de Janeiro, RJ CEP 20550-900, Brazil.
Email: andrehc@uerj.br

Funding information
Coordination for the Improvement of Higher Education Personnel (CAPES); Prociência Program (UERJ); National Council for Scientific and Technological Development (CNPq), Grant/Award Number: 310390/2019-2

Abstract

We extend a formulation of the heat exchanger design optimization with fouling modeling to consider the effect of fouling on hydraulics. A shell-side fouling model was added so the optimization can consider cases with fouling in the tube and shell sides. The focus is the design of heat exchangers with fouling behavior associated with a threshold model, like in crude preheat trains. We solve the optimization problem by using a newly proposed Set Trimming technique. We compare our results with the traditional approach of using fixed fouling factors and the previous approach of not considering the hydraulic impact of fouling. We conclude that considering the deposit thickness leads to more realistic results that are different than the ones obtained using the previous approaches. Moreover, we show that previous approaches can render designs with larger pressure drops than the maximum imposed by the constraints, as well as exchangers with higher areas.

KEYWORDS
heat transfer, optimization

1 | INTRODUCTION

The use of optimization techniques to design shell and tube heat exchangers has proven to be a valuable tool to replace the traditional trial-and-validation procedures, as discussed recently by Costa and Bagajewicz.[1] Several different mathematical programming approaches were investigated to address the design optimization problem, such as nonlinear programming (NLP),[2] mixed-integer nonlinear programming (MINLP),[3–5] mixed-integer linear programming (MILP),[6–8] and integer linear programming (ILP).[8] Different stochastic optimization methods were also explored to address the heat exchanger design problem, such as, simulated annealing,[9] genetic algorithms,[10] particle swarm optimization,[11] artificial bee colony,[12] and firefly algorithm.[13] Additionally, heuristic and enumeration techniques are also found in the literature related to the shell-and-tube heat exchanger design problem.[14,15]

All articles mentioned above include fouling effects in the design problem formulation in the traditional way of using fixed values of fouling factors, as available in the literature.[16] However, several models relate the fouling rate or the fouling factor to thermofluid dynamic variables, particularly, temperature, and velocity. For example, Wilson et al.[17,18] presented overviews of fouling rate models for crude oil streams based on the threshold concept. Additionally, the modification of the structure of the heat transfer surface can also mitigate the fouling problem.[19]

The usual approach to address fouling in the design using fixed fouling factors has important limitations,[20] ignoring the influence of the heat exchanger design on the fouling extent. To answer this challenge, several articles have investigated the interconnection between fouling modeling and heat exchanger design procedures for the case of crude preheat trains.[21–26] The design optimization with fouling modeling was also addressed for other systems by Caputo et al.,[27] Lemos et al.,[28] and Roy and Majumder.[29]

The analysis of the literature about heat exchanger design optimization indicates that few articles mentioned the hydraulic impact of fouling. Indeed, fouling reduces the overall heat transfer coefficient because of the presence of additional thermal resistance, but fouling also increases the pressure drop in the heat exchangers. According to

 © 2022 American Institute of Chemical Engineers.

Kakaç and Liu,[30] more heat exchangers are removed from service due to excessive pressure drop than due to insufficient heat transfer rate. The relation between the hydraulic impact of fouling and the design was considered by Butterworth[22] and Polley et al.[23,24]

Considering the limited attention that the hydraulic impact of fouling has received in previous design optimization studies, the objective of this article is to propose a procedure that not only encompasses a fouling model representing the thermal behavior of fouling, but also its hydraulic impact. The focus of our article is the design of heat exchangers in crude fractionation units, where fouling is an important operational issue.

We extend the model presented by Lemos et al.[21] to include the equations that relate the increase of the pressure drop with the thickness of the deposits.[31] While Lemos et al.[21] identified the optimal solution using mathematical programming, we explore here the utilization of Set Trimming, a new approach that uses inequality constraints one at a time to gradually reduce the search space.[1] The use of Set Trimming for the design optimization of shell and tube exchangers using a conventional representation of the fouling impact has been explored in great detail and compared to the use of rigorous linear models solved using MILP and ILP procedures by Lemos et al.[32]

The major focus of this study is to show that the thickness of the fouling deposits has a significant effect on the pressure drop. The proposed model can consider the presence of fouling in the tube-side, the shell-side, or in both sides simultaneously (or even in its absence at all). The most common situation observed in crude preheat trains is the crude oil flowing in the tube-side, where fouling occurs. Diaz-Bejarano et al.[33] mentioned that "negligible" fouling on the shell side as being the "most common case in refinery heat exchangers." However, in some equipment, fouling can also occur in the shell-side of crude preheat trains. Coletti et al.[34] remarked that fouling on the shell side takes place when the shell fluid is a "heavy petroleum fraction or if crude is switched to the shell-side for design reasons."

We remark that our approach is based on limit fouling values without considering the dynamic of fouling. For cases where fouling takes place on one side of the exchanger (tube or shell side), one can identify long-term values of fouling resistance. However, in cases where fouling takes place on both tube and shell sides, be it from the beginning for both sides or not, the final state can only be determined through a dynamic simulation. Because our approach is solely based on long-term values of fouling resistances, we choose to use upper bounds of the fouling resistance that expresses a limit value in these cases, adequate for design purposes.

The remainder of this article is organized as follows. Initially, the formulation of the heat exchanger design problem is discussed, including the modeling of the thermal and hydraulic aspects of fouling. Then, we discuss the Set Trimming technique applied to identify the global optimum solution. After that, the results of the proposed approach are compared with the conventional approach of designing with fixed fouling factor and with a design approach associated with fouling modeling but considering only its thermal impact. In the end, conclusions are presented.

2 | HEAT EXCHANGER DESIGN OPTIMIZATION

The shell and tube heat exchanger design problem consists of the minimization of the heat transfer area according to the available pressure drops. Alternative objective functions are the total annualized cost (TAC) or weight and detailed costing.[35] Here, we consider no phase change streams in a single E-shell type, where the tube-side and shell-side streams present a fouling behavior represented by a threshold model.[17,18]

The search space is composed of a set of design alternatives. Each solution candidate is defined by a set of values of the following design variables: inner and outer tube diameters (*dti* and *dte*), shell diameter (*Ds*), tube length (*L*), number of baffles (*Nb*), number of tube passes (*Ntp*), tube pitch ratio (*rp*), tube layout (*lay*), and baffle cut ratio (*Bc*). Because of its physical nature and/or commercial standards, the problem variables are assumed discrete.

We present next the objective function and the problem constraints. Model parameters are identified with a symbol ^ on top. The constraints associated with the fouling model, involving thermal and hydraulic equations are shown later.

2.1 | Objective function

The optimization seeks to identify the heat exchanger with the minimum area, therefore the objective function of the problem is represented by:

$$A = Ntt\,\pi\,dte\,L \tag{1}$$

where *Ntt* is the total number of tubes of the heat exchanger, defined according to a proper counting table[36] or equivalent equations.[30]

2.2 | Geometric constraints

The ratios L/Ds and lbc/Ds (*lbc* is the baffle spacing) are bounded[37] and the maximum unsupported span of tubes (*lbmax*) is bounded according to TEMA standards:

$$3\,Ds \le L \le 15\;Ds \tag{2}$$

$$0.2\,Ds \le lbc \le 1.0\;Ds \tag{3}$$

$$lbc \le 0.5\,lbmax \tag{4}$$

where *lbmax* depends on the material of the tube and the outer tube diameter.

2.3 | Velocity bounds

Flow velocities in the tube-side (*vt*) and shell-side (*vs*) must obey upper bounds to avoid vibration and erosion.

15475905, 2022, 5, Downloaded from https://aiche.onlinelibrary.wiley.com/doi/10.1002/aic.17586 by University Of Oklahoma, Wiley Online Library on [04/11/2023]. See the Terms and Conditions (https://onlinelibrary.wiley.com/terms-and-conditions) on Wiley Online Library for rules of use; OA articles are governed by the applicable Creative Commons License

$$vs \le \widehat{vsmax} \tag{5}$$

$$vt \le \widehat{vtmax} \tag{6}$$

Usually, lower bounds on velocities are also included to avoid solutions associated with excessive fouling, but the current approach can predict the impact of fouling through fouling rate models, therefore these constraints are not necessary in the current approach.

2.4 | Reynolds numbers bounds

Bounds on the Reynolds numbers in the tube-side (*Ret*) and shell-side (*Res*) are associated with the validity of the thermofluid dynamic correlations:

$$Res \le \widehat{Resmax} \tag{7}$$

$$Ret \le \widehat{Retmax} \tag{8}$$

2.5 | Pressure drop bounds

Pressure drops in the shell-side (ΔPs) and tube-side (ΔPt) must also be bounded:

$$\Delta Ps \le \widehat{\Delta Psdisp} \tag{9}$$

$$\Delta Pt \le \widehat{\Delta Ptdisp} \tag{10}$$

The tube-side pressure drop evaluation uses the Darcy–Weisbach equation[36] considering the presence of a deposit layer inside the tube and the shell-side pressure drop is evaluated by the Bell–Delaware method considering the presence of a deposit layer outside the tube (Figure 1). Both models correspond to the equations presented in Gonçalves et al.[7] adapted to encompass the presence of the corresponding fouling layer (see Supporting Information).

2.6 | Heat transfer rate constraint

According to the LMTD method:[38]

$$\widehat{Q} = U\,Areq\,\widehat{\Delta Tlm}\,F \tag{11}$$

where U is the overall heat transfer coefficient, $\widehat{\Delta Tlm}$ is the logarithmic mean temperature difference for the countercurrent configuration, and F is the correction factor of the mean temperature difference.

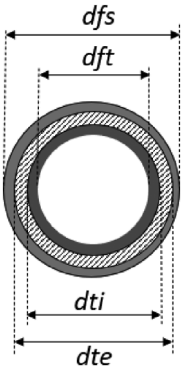

FIGURE 1 Cross section of a fouled tube

Thus, the heat transfer area of the exchanger must be higher than the required area, according to a design margin, called an "excess area" ($\widehat{Aexc}$):

$$A \ge \left(1 + \frac{\widehat{Aexc}}{100}\right) Areq \tag{12}$$

In turn, the expression of the overall heat transfer coefficient is:

$$U = \frac{1}{\frac{dte}{dti\,ht} + \frac{Rft\,dte}{dti} + \frac{dte\ln\left(\frac{dte}{dti}\right)}{\widehat{2\,ktube}} + \frac{1}{hs} + Rfs} \tag{13}$$

where ht and hs are the convective heat transfer coefficients for the tube-side and shell-side, respectively; $\widehat{ktube}$ is the thermal conductivity of the tube wall; Rft is the fouling resistance for the tube-side and Rfs, for the shell-side. The shell-side heat transfer coefficient is evaluated using the Bell–Delaware model. The evaluation of the tube-side heat transfer coefficient involves several correlations to encompass all flow regimes, as described in Supporting Information.

3 | FOULING MODEL

The proposed model considers the possibility of the presence of fouling in the tube-side and shell-side streams of the heat exchanger, with a behavior represented by a threshold model,[17,18] including the hydraulic impact of fouling. The threshold model is an approach widely employed to describe the fouling behavior on streams of crude preheat trains. Although the shell-side fouling is assumed negligible in most of the works dealing with preheat trains, which is a common situation,[33] here we also consider the possibility of its presence, as occur in some cases.[34]

The presentation of the fouling model below is organized in the following subsections: fouling hydraulic impact modeling, tube-side fouling model, shell-side fouling model, tube-side versus shell-side fouling models, and possible fouling behaviors for a given exchanger.

15475905, 2022, 5, Downloaded from https://aiche.onlinelibrary.wiley.com/doi/10.1002/aic.17586 by University Of Oklahoma, Wiley Online Library on [04/11/2023]. See the Terms and Conditions (https://onlinelibrary.wiley.com/terms-and-conditions) on Wiley Online Library for rules of use; OA articles are governed by the applicable Creative Commons License

3.1 | Fouling hydraulic impact

The increase of the pressure drop due to the accumulation of deposits can be caused by the following reasons: tube blockage, increase of surface roughness, and reduction of the free flow area due to the fouling layer.[31] We focus our model on the last contribution, illustrated in Figure 1, where the inner and outer tube diameters (*dti* and *dte*), the fouled inner diameter (*dft*), and the fouled outer diameter (*dfs*) are shown. In this section, we discuss how the fouling thickness (δft and δfs), hence *dft* ($dft = dti - 2\delta ft$) and *dfs* ($dfs = dte + 2\delta fts$), can be related to the fouling resistance.

We consider the fouling thickness and the fouling thermal conductivity to be uniform along the heat transfer area for both sides and for the shell-side we consider that fouling occurs on the outer tube surface and on the inner shell surface, impacting the clearances in the Bell–Delaware model. The complete model that takes it into account can be found in Supporting Information. There are models that investigated the spatial distribution of the fouling thickness along the heat transfer area which provides a more detailed description of the phenomenon,[34] but none of them were employed for heat exchanger design purposes.

Based on the above assumptions, the fouled overall heat transfer coefficient can be represented in the following two ways:

$$\frac{1}{U} = \frac{1}{hs} + Rfs + \frac{dte}{2\,\widehat{ktube}}\ln\left(\frac{dte}{dti}\right) + \frac{dte}{dti}Rft + \frac{dte}{dti}\frac{1}{ht} \tag{14}$$

$$\frac{1}{U} = \frac{dte}{(dte+2\delta fs)}\frac{1}{hsf} + \frac{dte}{2\,\widehat{kfs}}\ln\left(\frac{dte+2\delta fs}{dte}\right) + \frac{dte}{2\,\widehat{ktube}}\ln\left(\frac{dte}{dti}\right) + \frac{dte}{2\,\widehat{kft}}\ln\left(\frac{dti}{dti-2\delta ft}\right) + \frac{dte}{(dti-2\delta f)}\frac{1}{htf} \tag{15}$$

where *htf* and *hfs* are the heat transfer coefficients at the fouled conditions for tube-side and shell-side, $\widehat{kft}$ and $\widehat{kfs}$ are the fouling thermal conductivities for the tube-side and shell-side.

The expression in Equation (15) is equivalent to Equation (14), but instead of using a fouling resistance, it considers the effect of fouling through an explicit thermal resistance of the deposits layer. An additional consideration to make is that the values of *htf* and *ht* are different in a fouled condition: the value of *htf* is higher than *ht* due to the increase of the flow velocity associated with the reduction of the free flow diameter (*dft* < *dti*), the same can be said about the shell-side, *hsf* is higher than *hs*.

Because Equations (14) and (15) are equivalent and the first two terms of Equation (15) are related to the shell-side and the last two terms to the tube-side, we can write the following relations by matching the terms and isolating the fouling resistances:

$$Rfs = \frac{dte}{dfs}\frac{1}{hsf} + \frac{dte}{2\,\widehat{kfs}}\ln\left(\frac{dfs}{dte}\right) - \frac{1}{hs} \tag{16}$$

$$Rft = \frac{dti}{2\,\widehat{kft}}\ln\left(\frac{dti}{dft}\right) + \frac{dti}{dft}\frac{1}{htf} - \frac{1}{ht} \tag{17}$$

The same relation for the tube-side (Equation (17)) was obtained by Yeap et al.[31] when considering that the heat transfer coefficients are impacted by the fouling growth.

These relations between the fouling resistances and the fouled diameters allow describing the hydraulic impact of fouling, that is, the increase of the fouling resistance brings a reduction of the flow area leading to larger pressure drops.

3.2 | Tube-side fouling model

The threshold model represents the fouling rate as the difference between a formation rate (φ_D) and a suppression rate (φ_R):

$$\frac{dRft}{dt} = \varphi_D - \varphi_R \tag{18}$$

It is an open issue in the literature if the negative term in Equation (18) is a suppression term or a removal term.[39] The removal option implies that the fouling rate can be negative, that is, the fouling resistance can decrease during the heat exchanger operation. The suppression option considers that if the difference in Equation (18) becomes negative then the fouling rate becomes zero, without decrease of the fouling resistance. As mentioned above, we adopt here the latter option.[40]

Among the several options of threshold models,[17,18] without loss of generality, we use the threshold fouling model proposed by Polley et al.:[41]

$$\frac{dRft}{dt} = \widehat{\alpha t}\,Ret^{-0.8}\,\widehat{Prt}^{-0.33}\exp\left(\frac{-\widehat{Eat}}{\widehat{R}\,Tst}\right) - \widehat{\gamma t}\,Ret^{0.8} \tag{19}$$

where *Tst* is the surface temperature of the tube-side (the wall temperature in the clean exchanger and the deposit surface temperature in the fouled case); $\widehat{\alpha t}$, $\widehat{\gamma t}$, and $\widehat{Eat}$ are model empirical parameters; *Ret* is the Reynolds number; $\widehat{Prt}$ is the Prandlt number; and $\widehat{R}$ is the universal gas constant.

The fouling rate model can be described more compactly:

$$\frac{dRft}{dt} = \widehat{Aft}\,Ret^{-0.8}\exp\left(\frac{-\widehat{\psi ft}}{Tst}\right) - \widehat{Bft}\,Ret^{0.8} \tag{20}$$

where $\widehat{Aft} = \widehat{\alpha t}\,\widehat{Prt}^{-0.33}$, $\widehat{Bft} = \widehat{\gamma t}$ and $\widehat{\psi ft} = \frac{-\widehat{Eat}}{\widehat{R}}$.

According to the threshold model, if the suppression rate is higher than the formation rate, then no fouling occurs. Therefore, the model delimits two regions in terms of the surface temperature and fluid velocity: a no fouling region and a fouling region, as shown in Figure 2.

The wall temperature can be determined by considering the thermal circuit shown in Figure 3, for which we can write:

15475905, 2022, 5, Downloaded from https://aiche.onlinelibrary.wiley.com/doi/10.1002/aic.17586 by University Of Oklahoma, Wiley Online Library on [04/11/2023]. See the Terms and Conditions (https://onlinelibrary.wiley.com/terms-and-conditions) on Wiley Online Library for rules of use; OA articles are governed by the applicable Creative Commons License

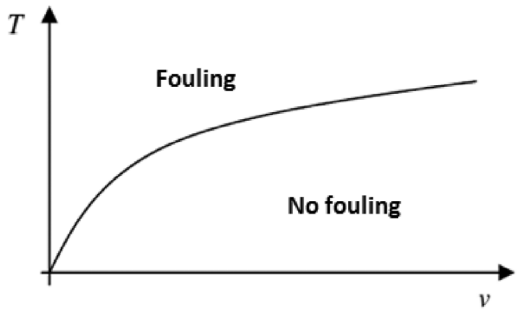

FIGURE 2 Threshold fouling

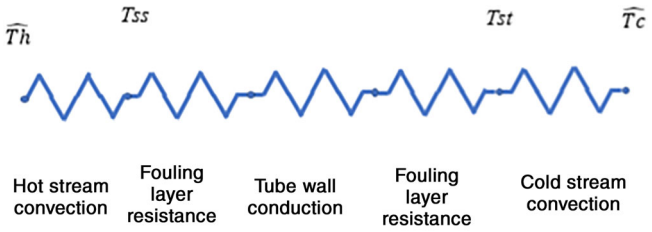

FIGURE 3 Thermal circuit between hot and cold streams

$$\frac{\widehat{Th}-Tst}{\frac{1}{hsf}+\frac{dte\,ln(dfs/dfte)}{2kfs}+\frac{dte\,ln(dte/dti)}{2ktube}+\frac{dte\,ln(dti/dft)}{2kft}}=\frac{Tst-\widehat{Tc}}{\frac{1}{htf}\left(\frac{dte}{dft}\right)} \quad (21)$$

where $\widehat{Th}$ and $\widehat{Tc}$ are the average temperatures of the hot and cold streams.

Thus, Tst is given by the following expression:

$$Tst=\frac{\left(\widehat{Th}-\widehat{Tc}\right)\frac{1}{htf}\left(\frac{dte}{dft}\right)}{\frac{1}{hsf}+\frac{dte\,ln(dfs/dfte)}{2kfs}+\frac{dte\,ln(dte/dti)}{2ktube}+\frac{dte\,ln(dti/dft)}{2kft}+\frac{1}{htf}\left(\frac{dte}{dft}\right)}+\widehat{Tc} \quad (22)$$

The no fouling condition in the tube-side takes place when the formation rate is smaller than or equal to the suppression rate, represented below for a null fouling resistance in the shell-side (e.g., at beginning of the operation, after a full cleaning of the heat exchanger):

$$\widehat{Aft}Ret^{-0.8}\exp\left(\frac{-\widehat{\psi ft}}{\frac{\left(\widehat{Th}-\widehat{Tc}\right)\frac{1}{ht}\left(\frac{dte}{dti}\right)}{\frac{1}{hs}+\frac{dte\,ln(dte/dti)}{2ktube}+\frac{1}{ht}\left(\frac{dte}{dti}\right)}+\widehat{Tc}}\right)\le\widehat{Bft}Ret^{0.8} \quad (23)$$

If there is fouling, the threshold model can also predict the asymptotic fouling condition (indicated here by the superscript ∞), which takes place when the formation and suppression rates become equivalent during the operation (represented below considering the presence of a known shell-side fouling):

$$\widehat{Aft}\exp\left(\frac{-\widehat{\psi ft}}{\frac{\left(\widehat{Th}-\widehat{Tc}\right)\frac{1}{htf}\left(\frac{dte}{dft}\right)}{\frac{1}{hsf}+\frac{dte\,ln(dfs/dfte)}{2kfs}+\frac{dte\,ln(dte/dti)}{2ktube}+\frac{dte\,ln(dti/dft)}{2kft}+\frac{1}{htf}\left(\frac{dte}{dft}\right)}+\widehat{Tc}}\right)=\widehat{Bft}(Ret^{\infty})^{1.6} \quad (24)$$

3.3 | Shell-side fouling model

The threshold model was originally developed for crude oil streams flowing in the tube-side.[17,18] Loyola-Fuentes and Smith[42,43] suggested the use of linear fouling for wax deposits, which is not amenable for threshold modeling as it does not exhibit finite long-term behavior. However, Diaz-Bejarano et al.[44] proposed the utilization of a threshold model for the modeling of the fouling rate in the shell-side. Therefore, we also adopted the same approach, assuming the validity of the Polley et al. model.[41] for the shell-side.

Applying an equivalent analysis for the shell-side as presented above for the tube-side yields the following set of equations.

The fouling rate model for the shell-side, analogous to Equation (20), is given by:

$$\frac{dRfs}{dt}=\widehat{Afs}Res^{-0.8}\exp\left(\frac{-\widehat{\psi fs}}{Tss}\right)-\widehat{Bfs}Res^{0.8} \quad (25)$$

The shell-side surface temperature, Tss can be calculated by (Figure 3):

$$Tss=\widehat{Th}-\frac{\left(\widehat{Th}-\widehat{Tc}\right)\frac{1}{hsf}}{\frac{1}{hsf}+\frac{dte\,ln(dfs/dfte)}{2kfs}+\frac{dte\,ln(dte/dti)}{2ktube}+\frac{dte\,ln(dti/dft)}{2kft}+\frac{1}{htf}\left(\frac{dte}{dft}\right)} \quad (26)$$

Therefore, the no fouling condition for the shell-side is (considering a clean tube-side condition):

$$\widehat{Afs}Res^{-0.8}\exp\left(\frac{-\widehat{\psi fs}}{\widehat{Th}-\frac{\left(\widehat{Th}-\widehat{Tc}\right)\frac{1}{hsf}}{\frac{1}{hs}+\frac{dte\,ln(dte/dti)}{2ktube}+\frac{1}{ht}\left(\frac{dte}{dti}\right)}}\right)\le\widehat{Bfs}Res^{0.8} \quad (27)$$

and the asymptotic fouling condition is:

$$\widehat{Afs}\exp\left(\frac{-\widehat{\psi fs}}{\widehat{Th}-\frac{\left(\widehat{Th}-\widehat{Tc}\right)\frac{1}{hsf}}{\frac{1}{hsf}+\frac{dte\,ln(dfs/dfte)}{2kfs}+\frac{dte\,ln(dte/dti)}{2ktube}+\frac{dte\,ln(dti/dft)}{2kft}+\frac{1}{htf}\left(\frac{dte}{dft}\right)}}\right)=\widehat{Bfs}(Res^{\infty})^{1.6} \quad (28)$$

15475905, 2022, 5, Downloaded from https://aiche.onlinelibrary.wiley.com/doi/10.1002/aic.17586 by University Of Oklahoma, Wiley Online Library on [04/11/2023]. See the Terms and Conditions (https://onlinelibrary.wiley.com/terms-and-conditions) on Wiley Online Library for rules of use; OA articles are governed by the applicable Creative Commons License

3.4 | Tube-side versus shell-side fouling model

The fouling behavior of the tube-side and shell-side streams depends on the interaction between both sides. Indeed, the presence of fouling on one side alters the surface temperature on the other side, and this affects the resultant fouling rate on the other side. Therefore, the tube-side and shell-side fouling models presented above must be analyzed together to identify the fouling status of a given heat exchanger.

The objective of this analysis is to identify which fouling condition will be present in the long-term in each stream according to the threshold model: no fouling or asymptotic fouling. This diagnosis involves an analysis of the initial fouling rates of the heat exchanger (assuming that both sides are clean) followed by a complementary analysis of the corresponding fouling condition in the long-term.

For a given heat exchanger, five fouling behavior alternatives can occur. Therefore, each heat exchanger design candidate will be classified into one of the subsets discussed in the next subsections. In some cases, it is not possible to diagnose the exact value of the long-term fouling resistance, and, alternatively, upper bound values are provided that can be employed as a fouling resistance limit for design purposes. The Supporting Information contains the detailed representation of the corresponding mathematical problems.

The analyses present in the following subsections assume that the tube-side stream is the cold stream (e.g., crude oil) and the shell-side stream is the hot stream (e.g., distillate cut). This is the most common allocation in crude preheat trains, but the same approach can be directly extended for the opposite stream allocation.

3.5 | Subset 1—Tube-side: no fouling/shell-side: no fouling

If the conditions expressed in Equations (23) and (27) are true, therefore tube-side and shell-side streams are in the no fouling condition at the beginning of the operation. Because no fouling layer is formed in both sides during the operation, the surfaces temperatures do not modify and the no fouling condition is present in the long-term.

3.6 | Subset 2—Tube-side: no fouling/shell-side: fouling

If the condition expressed in Equation (23) is true, but the condition expressed in Equation (27) is false, therefore there is no fouling in the tube-side at the beginning of the operation of the heat exchanger, but there is a positive fouling rate in the shell-side.

As time passes, the presence of fouling in the shell-side reduces the tube-side surface temperature. Therefore, the formation rate of fouling (φ_D in Equation (18)) is also reduced and the tube-side keeps the no fouling condition in the long-term. Based on the absence of fouling in the tube-side, it is possible to evaluate the shell-side fouling asymptotic thickness in terms of *dfs*, based on Equation (28) for $dtf = dti$ and $htf = ht$ (i.e., $Rft = 0$).

3.7 | Subset 3—Tube-side: fouling/shell-side: no fouling

If the condition expressed in Equation (23) is false, but the condition expressed in Equation (27) is true, therefore there is a positive fouling rate in the tube-side at the beginning of the operation of the heat exchanger, but there is a null fouling rate in the shell-side.

The accumulation of deposits in the tube-side contributes to the increase of the surface temperature on the shell-side. Therefore, the no-fouling condition may be displaced in the long term. The analysis presented below checks if the no-fouling condition remains in the long term.

Initially, the asymptotic fouling resistance in the tube-side, represented by the corresponding fouled diameter *dft* can be calculated using Equation (24) with $dfs = dte$ and $hsf = hs$ (i.e., $Rfs = 0$). Then, the check of the no fouling condition in the long-term can be tested through Equation (27), including the fouling terms associated to the value of *dft* already calculated. If this condition is true, the heat exchanger candidate presents asymptotic fouling in the tube-side and no fouling on the shell-side. Otherwise, there will be fouling on both sides and upper bounds on the fouling resistances can be calculated, as shown in the next subsection.

3.8 | Subset 4—Tube-side: fouling/shell-side: fouling

If the condition expressed in Equation (23) is false, but the condition expressed in Equation (27) is true, as shown in the previous case, but the no fouling condition is false in the long-term, it is not possible to directly diagnose the long-term fouling resistances in this case (the interruption of the fouling growth may be associated with a condition where the suppression rate is higher than the formation rate and a corresponding system of equations cannot be established). Alternatively, for design purposes, we evaluate upper bound values on the fouling resistances for the tube-side and shell-side streams, as presented below (in order to simplify the notation, we also identify the fouling resistance upper bound with the superscript ∞).

The upper bound on the fouling resistance in the tube-side can be calculated using Equation (24) assuming that there is no fouling in the shell-side and evaluating the shell-side heat transfer coefficient at the maximum velocity ($\widehat{vsmax}$). These assumptions are associated with the highest value of the tube-side surface temperature, which provides the desired upper bound on the tube-side fouling resistance. The solution of Equation (24) with these assumptions allows the evaluation of *dft* that is associated with the corresponding values of fouling thickness and fouling resistance.

The upper bound on the fouling resistance in the shell-side can be calculated using Equation (28) in an analogous approach, based on assumptions that the fouling in the tube-side corresponds to the upper bound evaluated in the previous paragraph and the tube side heat transfer coefficient is calculated using the flow velocity at the clean condition. These assumptions are associated with the highest

15475905, 2022, 5, Downloaded from https://aiche.onlinelibrary.wiley.com/doi/10.1002/aic.17586 by University Of Oklahoma, Wiley Online Library on [04/11/2023]. See the Terms and Conditions (https://onlinelibrary.wiley.com/terms-and-conditions) on Wiley Online Library for rules of use; OA articles are governed by the applicable Creative Commons License

value of the shell-side surface temperature, which provides an upper bound of the shell-side fouling resistance. The solution of Equation (28) with these assumptions allows the evaluation of *dfs* that is associated with the corresponding values of fouling thickness and fouling resistance.

3.9 | Subset 5—Tube-side: fouling/shell-side: fouling

If both conditions corresponding to Equations (23) and (27) at the beginning of the operation are false, therefore there are positive fouling rates in the tube-side and shell-side streams. However, similarly to the previous case, it is also not possible to directly diagnose the long-term fouling resistances. Therefore, the same procedure described above is applied to provide upper bounds on the fouling resistances for both streams.

3.10 | Maximum fouling

If the asymptotic fouling resistance is higher than a maximum fouling resistance one desires to tolerate, the maximum fouling resistance is then used in the design, that is:

$$Rft = \min\left(\widehat{Rft}^{max}, Rft^{\infty}\right) \tag{29}$$

$$Rfs = \min\left(\widehat{Rfs}^{max}, Rfs^{\infty}\right) \tag{30}$$

4 | OPTIMIZATION PROCEDURE

The proposed formulation of the heat exchanger design optimization is a mixed-integer nonlinear model and instead of solving it using an MINLP solver (e.g., DICOPT, SBB, BARON, etc.), we use a different approach: Set Trimming.[1]

Set Trimming is a procedure that employs the inequality problem constraints for reducing the number of available candidate solutions. Each constraint yields a partially feasible set of solution candidates that satisfies all problem constraints explored up to that point. Aiming at developing a more efficient procedure, the sequence of the constraints must consider the complexity of the calculations involved (it is considered more efficient to start exploring the simpler constraints and only to apply the more complex constraints, presumably more time consuming, at the end when the number of candidate solutions is smaller; this matter of knowing a priori the order is still under investigation, but the answer can be obtained experimenting). If all constraints are applied, the resultant set is the set of feasible candidates and, therefore, the identification of the optimal solution can be done by simple inspection or application of an enumeration procedure.

In our case, the set of discrete design variable values (*dti* and *dte*, *Ds*, *L*, *Nb*, *Npt*, *rp*, *lay*, and *Bc*) is the ones that represent all the degrees of freedom. Because the evaluation of the objective function is direct, the optimal solution is obtained by inspection. The continuous variables are evaluated from the design variables using the equality constraints.

Figure 4 shows the sequence of trimmings to identify the feasible heat exchangers in a given set of candidates. Examples of successful application of Set Trimming for optimization of thermal equipment design can be found in Lemos et al.[32] and Nahes et al.[45]

The search space corresponds to the set of heat exchanger candidates composed of all possible combinations of the available discrete values of the design variables. This set is partitioned into five subsets according to the corresponding fouling behavior described in the previous section. The identification of the candidates that belong to each subset and the associated evaluation of the fouling resistances may involve a considerable numerical effort. Therefore, aiming at reducing the computational time, instead of identifying the heat exchangers of all subsets simultaneously, the proposed optimization procedure identifies the heat exchangers that belong to each subset sequentially. After the identification of a given subset, the Set Trimming procedure is applied to this subset, thus finding the heat exchanger candidates in this subset with the smallest area that is feasible (if exists at least a single feasible candidate). Then, the candidates of this subset are eliminated from the search and the area of the best feasible candidate of this subset becomes the new incumbent. Finally, after the update of the incumbent, the heat exchangers in the remaining search space with area higher than the incumbent area are also eliminated. When the last subset is explored, the search stops and the optimal heat exchanger is the incumbent. Figure 5 illustrates the optimization procedure. It is important to observe in Figure 5 the application of a Set Trimming procedure to the entire search space without fouling, before the

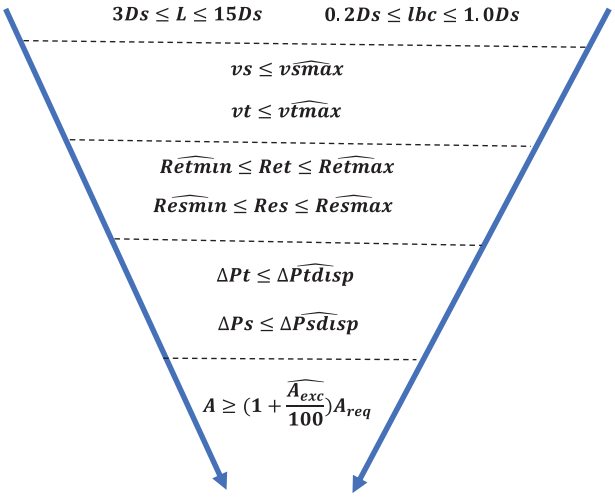

FIGURE 4 Identification of feasible heat exchanger candidates through Set Trimming

15475905, 2022, 5, Downloaded from https://aiche.onlinelibrary.wiley.com/doi/10.1002/aic.17586 by University Of Oklahoma, Wiley Online Library on [04/11/2023]. See the Terms and Conditions (https://onlinelibrary.wiley.com/terms-and-conditions) on Wiley Online Library for rules of use; OA articles are governed by the applicable Creative Commons License

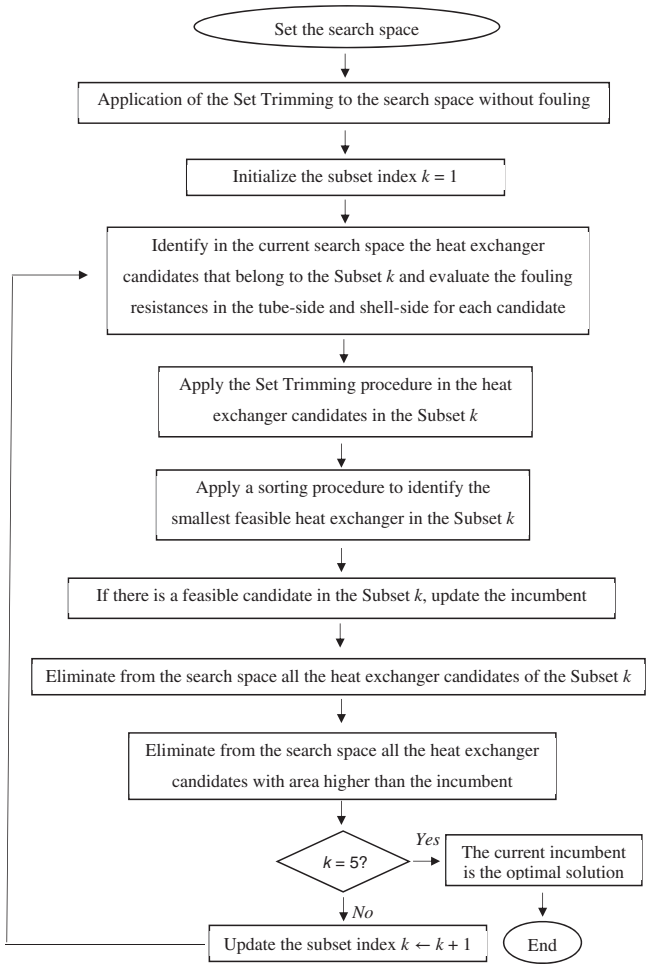

FIGURE 5 Optimization algorithm

application of the loop associated with the analysis of each subset. The objective of this step is to eliminate all heat exchanger candidates that are not feasible even in clean conditions. This step allows a decrease of the computational effort, because it reduces the number of heat exchangers to be tested in the steps of the identification of the subsets associated with different fouling patterns. Because all heat exchangers that are not geometrically feasible (Equations (2)–(4)) are excluded in this Set Trimming step, the application of Set Trimming in the subsets does not include these constraints (Figure 5).

5 | RESULTS

We solved four examples using the proposed approach, they are based on the same data, where only the fouling rate model parameters are varied. The examples are associated with optimal solutions related to different subsets mentioned in the Fouling Model Section. The physical properties of the streams and the characteristics of the thermal service of the examples are presented in Tables 1 and 2. These values were adapted from a real crude preheat train, where the cold stream, crude oil, flows in the tube-side and the hot stream flows in the shell-side. The discrete options of the geometric variables are

TABLE 1 Physical properties

	Cold stream	Hot stream
Density (kg/m^3)	768.9	898.0
Viscosity (Pa s)	5.36×10^{-4}	1.87×10^{-3}
Thermal conductivity (W/m K)	0.09	0.13
Heat capacity (J/kg K)	2754	2742

TABLE 2 Thermal service

	Cold stream	Hot stream
Mass flow rate (kg/s)	91.9	40.0
Inlet temperature (°C)	308.4	363.8
Outlet temperature (°C)	325.0	325.4

TABLE 3 Alternatives of discrete values of the design variables

Variable	Values
Tube outer diameter (m)	0.01905, 0.02540, 0.03175, 0.03810, 0.05080
Tube length (m)	3.6585, 4.8768, 6.0976
Number of baffles	13–20
Number of tube passes	1, 2, 4
Tube pitch ratio	1.25, 1.33, 1.50
Shell diameter (m)	0.9398, 0.9906, 1.0668, 1.1430, 1.2192, 1.3716
Tube layout	1 = square, 2 = triangular
Baffle cut	0.15, 0.20, 0.25

presented in Table 3. This results in 38,880 candidates. The thermal conductivity of the fouling layer on the tube-side is 1.4 W/(m K) and on the shell-side is 1.0 W/(m K), within the range reported in the literature for this parameter.[46] The thermal conductivity of the tube wall is 50 W/(m K) and the tube wall thickness is 0.001225 m. The maximum pressure drop allowable for all streams is 50 kPa for Examples 1–3, and 30 kPa for Example 4. The maximum flow velocities in the tube-side and shell-side are 3 and 2 m/s, respectively.

The design based on a fixed fouling resistance employs the values suggested by TEMA[16] (7.04×10^{-4} m^{2}K/W for the tube-side and 5.3×10^{-4} for the shell-side). These values are also used as the maximum fouling resistance allowed in the proposed design procedure ($\widehat{Rf}t^{max}$ and $\widehat{Rf}s^{max}$). The values of the empirical parameters of the fouling rate model in each example are displayed in Table 4.

All the examples were solved using the GAMS software in a computer with Intel Core i7 processor with 16 Mb of RAM memory. The solutions of the auxiliary mixed-integer nonlinear models were obtained using the solver SBB (the solver DICOPT was also tested, but it presented convergence limitations for this problem). Whenever the results pointed to different heat exchangers with the same area, but different number of baffles or baffle cut, only the one with the smallest values is portrayed. The computational times associated with the design optimization using fixed fouling resistances for all examples

15475905, 2022, 5, Downloaded from https://aiche.onlinelibrary.wiley.com/doi/10.1002/aic.17586 by University Of Oklahoma, Wiley Online Library on [04/11/2023]. See the Terms and Conditions (https://onlinelibrary.wiley.com/terms-and-conditions) on Wiley Online Library for rules of use; OA articles are governed by the applicable Creative Commons License

TABLE 4 Fouling rate model parameters

	Example 1	Example 2	Example 3	Example 4
αt (m^2 K/J)	0.2798	0.2798	0.2798	0.2798
γt (m^2 K/J)	4.17×10^{-13}	4.17×10^{-13}	4.17×10^{-13}	4.17×10^{-13}
Eat (J/mol)	48,000	48,000	38,000	45,000
αs (m^2 K/J)	0.2798	0.2798	0.2798	0.2798
γs (m^2 K/J)	4.17×10^{-12}	4.17×10^{-12}	4.17×10^{-11}	4.17×10^{-12}
Eas (J/mol)	48,000	41,000	48,000	40,000

TABLE 5 Example 1—Optimal values of the design variables

Variable	Proposed approach	Fouling model ignoring hydraulic impact	Fixed fouling resistance
Area (m^2)	322.1	322.1	756.5
Tube outer diameter (m)	0.0254	0.0254	0.01905
Tube length (m)	6.0976	6.0976	6.0976
Number of baffles	20	20	13
Number of tube passes	4	4	4
Tube pitch ratio	1.25	1.25	1.25
Shell diameter (m)	0.9398	0.9398	1.2192
Tube layout	1	1	1
Baffle cut	0.15	0.15	0.15

were about 2 s. The corresponding computational times for the approaches based on fouling modeling were larger in all examples, with the exception of Example 1.

Example 1. Tube-side: no fouling/shell-side: no fouling

The comparison of the optimal solutions using the proposed approach and the previous models are shown in Tables 5 and 6.

The optimal solutions obtained using the proposed approach and the model that ignores the hydraulic impact of fouling were the same. This equivalence occurred because the optimal heat exchanger is inside in the no fouling region for both streams. However, using the traditional approach, with the fixed fouling resistances from TEMA, the area of the heat exchanger was 134% higher than the proposed approach. This result demonstrates the advantage of using a fouling model in the design procedure since the fixed fouling resistances penalized the heat exchanger area of the solution, but the other two approaches could find a heat exchanger solution where fouling does not happen, which allows a reduction of the heat transfer surface.

Example 2. Tube-side: no fouling/shell-side: fouling

Tables 7 and 8 display the results obtained for the different approaches, it is important to notice that the value of tube-side and shell-side pressure drop displayed for the proposed approach already considers the hydraulic impact of fouling, while the other two do not. The problem was solved in 13 s using the Set Trimming proposed approach and in 24 s ignoring the hydraulic impact. The large difference of the computational times between the approaches that employ the fouling model and the approach based on fixed fouling resistances is explained by the demand to solve a considerable number of auxiliary mixed integer nonlinear models (however, the corresponding total computational times are still relatively low).

The result using the proposed approach led to a no fouling condition in the tube-side and a fouling condition in the shell-side, where the shell-side fouling resistance is the maximum one (5.3×10^{-4} m^2K/W), associated with a fouled inner diameter equal to 1.01 mm. The optimal heat transfer area of the traditional approach based on fixed fouling resistances is 55% higher. The identification of an optimal heat exchanger in the no fouling region in the tube-side using the fouling model allows a reduction of the heat transfer area. The design approach, which ignores the hydraulic impact identified a heat exchanger with the same area of the proposed approach, because the additional pressure drop associated with the fouling layer did not exclude this option from the feasible region.

Example 3. Tube-side: fouling/shell-side: no fouling

The results for the proposed new approach and the other two approaches are displayed in Tables 9 and 10.

15475905, 2022, 5, Downloaded from https://aiche.onlinelibrary.wiley.com/doi/10.1002/aic.17586 by University Of Oklahoma, Wiley Online Library on [04/11/2023]. See the Terms and Conditions (https://onlinelibrary.wiley.com/terms-and-conditions) on Wiley Online Library for rules of use; OA articles are governed by the applicable Creative Commons License

TABLE 6 Example 1—Optimal values of the thermofluid dynamic variables

Variable	Proposed approach	Fouling model ignoring hydraulic impact	Fixed fouling resistance
Shell-side pressure drop (kPa)	35.3	35.3	13.9
Tube-side pressure drop (kPa)	38.11	38.11	21.3
Shell-side heat transfer coefficient (W/m^2K)	1018.7	1018.7	791.9
Tube-side heat transfer coefficient (W/m^2K)	2319.8	2319.8	1526.1
Overall heat transfer coefficient (W/m^2K)	673.6	673.6	296.0
Shell-side velocity (m/s)	0.78	0.78	0.40
Tube-side velocity (m/s)	1.74	1.74	1.07
Tube-side fouling resistance (m^2K/W)	0	0	7.04×10^{-4}
Shell-side fouling resistance (m^2K/W)	0	0	5.3×10^{-4}

TABLE 7 Example 2—Optimal values of the design variables

Variable	Proposed approach	Fouling model ignoring hydraulic impact	Fixed fouling resistance
Area (m^2)	487.9	487.9	756.5
Tube outer diameter (m)	0.01905	0.01905	0.01905
Tube length (m)	6.0976	6.0976	6.0976
Number of baffles	13	13	17
Number of tube passes	4	4	4
Tube pitch ratio	1.25	1.25	1.25
Shell diameter (m)	0.9906	0.9906	1.2192
Tube layout	1	1	1
Baffle cut	0.15	0.15	0.15

TABLE 8 Example 2—Optimal values of the thermofluid dynamic variables

Variable	Proposed approach	Fouling model ignoring hydraulic impact	Fixed fouling resistance
Shell-side pressure drop (kPa)	39.0	18.6	23.2
Tube-side pressure drop (kPa)	47.4	47.4	21.3
Shell-side heat transfer coefficient (W/m^2K)	942.2	942.2	833.2
Tube-side heat transfer coefficient (W/m^2K)	2273.6	2273.6	1526.1
Overall heat transfer coefficient (W/m^2K)	366.9	366.9	301.5
Shell-side velocity (m/s)	0.49	0.49	0.52
Tube-side velocity (m/s)	1.65	1.65	1.07
Tube-side fouling resistance (m^2K/W)	0	0	7.04×10^{-4}
Shell-side fouling resistance (m^2K/W)	5.3×10^{-4}	5.3×10^{-4}	5.3×10^{-4}

The proposed approach and the approach ignoring the hydraulic impact solved the design problem in about 60 s for this example.

Our model renders an area approximately 20% smaller than the area found using fixed fouling resistances. The traditional approach considered a fixed shell-side fouling resistance equal to 5.3×10^{-4} m^2K/W, while the proposed approach rendered a solution in the no fouling region for the shell-side, explaining the difference between the results. The tube-side fouling resistance in the optimal heat exchanger using the proposed approach is associated with a fouling layer thickness of 2.25 mm. The approach based on the fouling modeling that does not consider the hydraulic impact attained a heat exchanger area 5.8% smaller than the one found using the proposed approach. However, the evaluation of this heat exchanger considering the hydraulic impact of fouling yields a pressure drop of 65 kPa. It is important to observe that the maximum pressure drop is 50 kPa, therefore these values indicate that this design solution will violate the pressure drop constraint due to the reduction of the flow area in the tube-side caused by the fouling layer.

15475905, 2022, 5, Downloaded from https://aiche.onlinelibrary.wiley.com/doi/10.1002/aic.17586 by University Of Oklahoma, Wiley Online Library on [04/11/2023]. See the Terms and Conditions (https://onlinelibrary.wiley.com/terms-and-conditions) on Wiley Online Library for rules of use; OA articles are governed by the applicable Creative Commons License

TABLE 9 Example 3—Optimal values of the design variables

Variable	Proposed approach	Fouling model ignoring hydraulic impact	Fixed fouling resistance
Area (m^2)	605.0	570.0	756.5
Tube outer diameter (m)	0.01905	0.01905	0.01905
Tube length (m)	4.8768	6.0976	6.0976
Number of baffles	14	13	17
Number of tube passes	4	4	4
Tube pitch ratio	1.25	1.25	1.25
Shell diameter (m)	1.2192	1.0668	1.2192
Tube layout	1	1	1
Baffle cut	0.15	0.15	0.15

TABLE 10 Example 3—Optimal values of the thermofluid dynamic variables

Variable	Proposed approach	Fouling model ignoring hydraulic impact	Fixed fouling resistance
Shell-side pressure drop (kPa)	20.8	16.8	23.2
Tube-side pressure drop (kPa)	32.5	35.7	21.3
Shell-side heat transfer coefficient (W/m^2K)	838.9	887.0	833.2
Tube-side heat transfer coefficient (W/m^2K)	1526.1	1974.2	1526.1
Overall heat transfer coefficient (W/m^2K)	360.0	393.3	301.5
Shell-side velocity (m/s)	0.54	0.46	0.52
Tube-side velocity (m/s)	1.38	1.83	1.07
Tube-side fouling resistance (m^2K/W)	7.04×10^{-4}	7.04×10^{-4}	7.04×10^{-4}
Shell-side fouling resistance (m^2K/W)	0	0	5.3×10^{-4}

TABLE 11 Example 4—Optimal values of the design variables

Variable	Proposed approach	Fouling model ignoring hydraulic impact	Fixed fouling resistance
Area (m^2)	968.5	756.5	756.5
Tube outer diameter (m)	0.01905	0.01905	0.01905
Tube length (m)	6.0976	6.0976	6.0976
Number of baffles	13	13	13
Number of tube passes	4	4	4
Tube pitch ratio	1.25	1.25	1.25
Shell diameter (m)	1.3716	1.2192	1.2192
Tube layout	1	1	1
Baffle cut	0.25	0.15	0.15

Example 4. Tube-side: fouling/shell-side: fouling

All the results of Example 4 are displayed in Tables 11 and 12, the proposed approach solved this example in about 83 s and the model ignoring the hydraulic impact solved it in about 75 s.

In this example, the area found with the proposed model is larger than the area found by the other two models. The solution for the other models is not feasible when considering the hydraulic impact of fouling, the pressure drops are 39.5 kPa for the tube-side and 34.5 kPa for the shell-side, both values are larger than the maximum allowable pressure drop of 30 kPa. The fouling thickness evaluated using the proposed approach is 2.27 and 1.31 mm for the tube and shell-side, respectively.

15475905, 2022, 5, Downloaded from https://aiche.onlinelibrary.wiley.com/doi/10.1002/aic.17586 by University Of Oklahoma, Wiley Online Library on [04/11/2023]. See the Terms and Conditions (https://onlinelibrary.wiley.com/terms-and-conditions) on Wiley Online Library for rules of use; OA articles are governed by the applicable Creative Commons License

TABLE 12 Example 3—Optimal values of the thermofluid dynamic variables

Variable	Proposed approach	Fouling model ignoring hydraulic impact	Fixed fouling resistance
Shell-side pressure drop (kPa)	29.4	13.9	13.9
Tube-side pressure drop (kPa)	25.7	21.3	21.3
Shell-side heat transfer coefficient (W/m^2K)	650.3	791.9	791.9
Tube-side heat transfer coefficient (W/m^2K)	1217.5	1526.1	1526.1
Overall heat transfer coefficient (W/m^2K)	398.9	490.0	490.0
Shell-side velocity (m/s)	0.36	0.40	0.40
Tube-side velocity (m/s)	1.09	1.38	1.38
Tube-side fouling resistance (m^2K/W)	7.04×10^{-4}	$7.04 \cdot 10^{-4}$	$7.04 \cdot 10^{-4}$
Shell-side fouling resistance (m^2K/W)	5.3×10^{-4}	$5.3 \cdot 10^{-4}$	$5.3 \cdot 10^{-4}$

6 | CONCLUSIONS

This article presented a new optimization algorithm based on the Set Trimming strategy to solve the heat exchanger design optimization problem considering the hydraulic impact of fouling. The proposed model can solve the heat exchanger design problem for crude preheat trains with the crude oil flowing in the tube-side and the distillate flowing in the shell-side. The proposed approach can consider the impact of fouling on both sides. However, the main ideas explored here can also be extended for other systems.

The examples where the performance of the proposed approach was tested in comparison of alternative solutions involving the fouling modeling that ignores the hydraulic impact and fixed fouling resistances showed that:

1. The inclusion of the fouling modeling in the design can identify solutions with a considerable reduction of the heat transfer area because allows the optimization procedure to identify heat exchanger alternatives that mitigate the fouling problem (e.g., solutions in the no fouling region). The relation between fouling rate and the thermofluid dynamic conditions can be explored not only in the design phase, as presented in the current article, but also in the analysis of the operation of the exchanger.[47,48]
2. The hydraulic impact of fouling can increase the pressure drop due to the reduction of the free flow area. The exclusion of this effect in the design problem may yield solutions with higher pressure drops than the limits imposed by the designer. The proposed approach, despite the higher complexity of the mathematical model, can overcome this problem, identifying optimal solutions that obey the pressure drop constraints, even at the fouled conditions observed during the process operation.

ACKNOWLEDGMENTS

André L. H. Costa thanks the National Council for Scientific and Technological Development (CNPq) for the research productivity fellowship (Process 310390/2019-2) and the financial support of the Prociência Program (UERJ). Julia C. Lemos thanks the Coordination for the Improvement of Higher Education Personnel (CAPES) for the postdoctoral fellowship through the PNPD Program. Miguel Bagajewicz thanks the scholarship of visiting researcher from UERJ.

AUTHOR CONTRIBUTIONS

Julia Lemos: Conceptualization (supporting); investigation (supporting); methodology (supporting); software (lead); writing – original draft (supporting); writing – review and editing (supporting). **André Costa:** Conceptualization (equal); investigation (equal); methodology (equal); supervision (equal); writing – original draft (equal); writing – review and editing (equal). **Miguel J Bagajewicz:** Conceptualization (equal); investigation (equal); methodology (equal); writing – original draft (equal); writing – review and editing (equal).

DATA AVAILABILITY STATEMENT

The data that supports the findings of this study are available in the supporting information of this article.

ORCID

André L. H. Costa https://orcid.org/0000-0001-9167-8754
Miguel J. Bagajewicz https://orcid.org/0000-0003-2195-0833

NOTATION

A	area (m^2)
$\widehat{Afs}$	fouling model parameter shell-side (m^2K/J)
$\widehat{Aft}$	fouling model parameter tube-side (m^2K/J)
$\widehat{Aexc}$	excess area (percentage)
$Areq$	required area (m^2)
Bc	baffle cut
$\widehat{Bfs}$	fouling model parameter shell-side (m^2K/J)
$\widehat{Bft}$	fouling model parameter tube-side (m^2K/J)
dfs	shell-side fouled diameter (m)
dft	tube -side fouled diameter (m)
dte	outer tube diameter (m)
dti	inner tube diameter (m)
Ds	shell diameter (m)
Ea	activation energy (J/mol)
F	LMTD correction factor (dimensionless)
hs	convective heat transfer coefficient on shell-side (W/m^2K)

15475905, 2022, 5, Downloaded from https://aiche.onlinelibrary.wiley.com/doi/10.1002/aic.17586 by University Of Oklahoma, Wiley Online Library on [04/11/2023]. See the Terms and Conditions (https://onlinelibrary.wiley.com/terms-and-conditions) on Wiley Online Library for rules of use; OA articles are governed by the applicable Creative Commons License

ht	convective heat transfer coefficient on tube-side (W/m^2K)
hsf	fouled convective heat transfer coefficient on shell-side (W/m^2K)
htf	fouled convective heat transfer coefficient on tube-side (W/m^2K)
$\widehat{kfs}$	thermal conductivity of shell-side fouling (W/m K)
$\widehat{kft}$	thermal conductivity of tube-side fouling (W/m K)
$\widehat{ktube}$	thermal conductivity of the tube (W/m K)
L	tube length (m)
lay	layout of the heat exchanger
lbc	baffle spacing (m)
lbmax	maximum baffle spacing (m)
Nb	number of baffles
Npt	number of tube passes
Ntt	total number of tubes
$\widehat{Prt}$	Prandtl number of the tube-side stream (dimensionless)
$\widehat{Q}$	heat load (W)
R	ideal gas constant (J/mol K)
Ret	Reynolds number of the tube-side stream (dimensionless)
$\widehat{Retmax}$	maximum Reynolds number of the tube-side stream (dimensionless)
$\widehat{Resmax}$	maximum Reynolds number of the tube-side stream (dimensionless)
Rfs	fouling resistance on shell-side (m^2K/W)
Rft	fouling resistance on tube-side (m^2K/W)
$\widehat{Rfs}^{max}$	maximum fouling resistance on shell-side (m^2K/W)
$\widehat{Rft}^{max}$	maximum fouling resistance on tube-side (m^1K/W)
rp	tube pitch ratio
$\widehat{Tc}$	cold side average temperature (K)
$\widehat{Th}$	hot side average temperature (K)
Tss	surface temperature shell-side (K)
Tst	surface temperature tube-side (K)
U	overall heat transfer coefficient (W/m^2 K)
vs	shell-side flow velocity (m/s)
$\widehat{vsmax}$	maximum shell-side flow velocity (m/s)
vt	tube-side flow velocity (m/s)
$\widehat{vtmax}$	maximum tube-side flow velocity (m/s)

GREEK LETTERS

αs	fouling model parameter shell-side (m^2K/J)
αt	fouling model parameter tube-side (m^2K/J)
γs	fouling model parameter shell-side (m^2K/J)
γt	fouling model parameter tube-side (m^2K/J)
δfs	shell-side fouling thickness (m)
δft	tube-side fouling thickness (m)
ΔPs	pressure drop on shell-side (Pa)
$\Delta\widehat{Psdisp}$	available pressure drop on shell-side (Pa)
ΔPt	pressure drop on tube-side (Pa)
$\Delta\widehat{Ptdisp}$	available pressure drop on tube-side (Pa)
$\Delta\widehat{Tlm}$	logarithmic mean temperature difference (°C)
$\widehat{\psi fs}$	threshold model parameter shell-side (K)
$\widehat{\psi ft}$	threshold model parameter tube-side (K)
φ_D	fouling formation rate
φ_R	fouling suppression rate

ORCID

André L. H. Costa https://orcid.org/0000-0001-9167-8754

Miguel J. Bagajewicz https://orcid.org/0000-0003-2195-0833

REFERENCES

1. Costa ALH, Bagajewicz MJ. 110th anniversary: on the departure from heuristics and simplified models toward globally optimal design of process equipment. *Ind Eng Chem Res*. 2019;58:18684-18702.
2. Jegede FO, Polley GT. Optimum heat exchanger design. *Chem Eng Res Des*. 1992;70(A2):133-141.
3. Mizutani FT, Pessoa FLP, Queiroz EM, Hauan S, Grossmann IE. Mathematical programming model for heat-exchanger network synthesis including detailed heat-exchanger designs. *Ind Eng Chem Res*. 2003; 42:4009-4018.
4. Ponce-Ortega JM, Serna-González M, Salcedo-Estrada LI, Jiménez-Gutiérrez AA. Minimum-investment design of multiple shell and tube heat exchangers using a MINLP formulation. *Chem Eng Res Des*. 2006; 84:905-910.
5. Ravagnani MASS, Caballero JA. A MINLP model for rigorous design of shell and tube heat exchangers using the TEMA standards. *Chem Eng Res Des*. 2007;85:1423-1435.
6. Gonçalves CO, Costa ALH, Bagajewicz MJ. Shell and tube heat exchanger design using mixed-integer linear programming. *AIChE J*. 2017;63:1907-1922.
7. Gonçalves CO, Costa ALH, Bagajewicz MJ. Linear method for the design of shell and tube heat exchangers using the Bell–Delaware method. *AIChE J*. 2019;65:e16602.
8. Gonçalves CO, Costa ALH, Bagajewicz MJ. Alternative mixed-integer linear programming formulations for shell and tube optimal design. *Ind Eng Chem Res*. 2017;56:5970-5979.
9. Chaudhuri PD, Diwekar UM. An automated approach for the optimal design of heat exchangers. *Ind Eng Chem Res*. 1997;36:3685-3693.
10. Ponce-Ortega JM, Serna-González M, Jiménez-Gutiérrez A. Use of genetic algorithms for the optimal design of shell-and-tube heat exchangers. *Appl Therm Eng*. 2009;29:203-209.
11. Ravagnani MASS, Silva AP, Biscaia EC, Caballero JA. Optimal design of shell-and-tube heat exchangers using particle swarm optimization. *Ind Eng Chem*. 2009;48:2927-2935.
12. Sahin AS, Kılıç B, Kılıç U. Design and economic optimization of shell and tube heat exchangers using artificial Bee Colony (ABC) algorithm. *Energ Conver Manage*. 2011;52:3356-3362.
13. Mohanty DK. Application of firefly algorithm for design optimization of a shell and tube heat exchanger from economic point of view. *Int J Therm Sci*. 2016;102:228-238.
14. Ravagnani MASS, Silva AP, Andrade AL. Detailed equipment design in heat exchanger networks synthesis and optimization. *Appl Therm Eng*. 2003;23:141-151.
15. Costa ALH, Queiroz EM. Design optimization of shell-and-tube heat exchangers. *Appl Therm Eng*. 2008;28:1798-1805.
16. TEMA. *Standards of the Tubular Exchangers Manufactures Association*. 9th ed. Tubular Exchanger Manufactures Association; 2007.
17. Wilson DI, Polley GT, S. J. Pugh. Ten years of Ebert, Panchal and the 'threshold fouling' concept. Proceedings of International Conference Heat Exchanger Fouling and Cleaning—2005. Vol RP2. Kloster Irsee, Germany; 2005: 25–36.
18. Wilson DI, Ishiyama EM, Polley GT. Twenty years of Ebert and Panchal - what next? *Heat Transf Eng*. 2017;38:669-680.
19. Chambon A, Anxionnaz-Minvielle Z, Cwicklinski G, Guintrand N, Buffet A. Shell-and-tube heat exchanger geometry modification: an efficient way to mitigate fouling. *Heat Transf Eng*. 2020;41:170-177.

15475905, 2022, 5, Downloaded from https://aiche.onlinelibrary.wiley.com/doi/10.1002/aic.17586 by University Of Oklahoma, Wiley Online Library on [04/11/2023]. See the Terms and Conditions (https://onlinelibrary.wiley.com/terms-and-conditions) on Wiley Online Library for rules of use; OA articles are governed by the applicable Creative Commons License

20. Shilling RL. Fouling and uncertainty margins in tubular heat exchanger design: an alternative. *Heat Transfer Eng*. 2012;33:1094-1104.
21. Lemos JC, Costa ALH, Bagajewicz M. Globally optimal linear approach to the design of heat exchangers using threshold fouling modeling. *AIChE J*. 2018;64:2089-2102.
22. Butterworth D. Design of shell-and-tube heat exchangers when the fouling depends on local temperature and velocity. *Appl Therm Eng*. 2002;22:789-801.
23. Polley GT, Wilson DI, Yeap BL, Pugh SJ. Use of crude oil threshold data in heat exchanger design. *Appl Therm Eng*. 2002;22:763-776.
24. Polley GT, Fuentes AM, Pugh SJ. Design of shell-and-tube heat exchangers to achieve a specified operating period in refinery preheat trains. *Heat Transfer Eng*. 2011;32:314-319.
25. Nakao A, Valdman A, Costa ALH, Bagajewicz MJ, Queiroz EM. Incorporating fouling modeling into shell-and-tube heat exchanger design. *Ind Eng Chem Res*. 2017;56:4377-4385.
26. Utami E, Malwindasari A, Biyanto TR. Optimization of geometries shell and tube heat exchanger to minimize fouling resistance by utilizing Polley threshold model. AIP Conference Proceedings. 2019; 2088: 020039.
27. Caputo AC, Pelagagge PM, Salini P. Joint economic optimization of heat exchanger design and maintenance policy. *Appl Therm Eng*. 2011;31:1381-1392.
28. Lemos JC, Costa ALH, Bagajewicz MJ. Linear method for the design of shell and tube heat exchangers including fouling modeling. *Appl Therm Eng*. 2017;125:1345-1353.
29. Roy U, Majumder M. Economic optimization and energy analysis in shell and tube heat exchanger by meta-heuristic approach. *Vacuum*. 2019;166:413-418.
30. Kakaç S, Liu H. *Heat Exchangers – Selection, Rating and Thermal Design*. CRC Press; 2002.
31. Yeap BL, Wilson DI, Polley GT, Pugh SJ. Mitigation of crude oil refinery heat exchanger fouling through retrofits based on thermo-hydraulic fouling models. *Chem Eng Res Des*. 2004;82:53-71.
32. Lemos JC, Costa ALH, Bagajewicz MJ. Set trimming procedure for the design optimization of shell and tube heat exchangers. *Ind Eng Chem Res*. 2020;59:14048-14054.
33. Diaz-Bejarano E, Coletti F, Macchietto S. A model-based method for visualization, monitoring, and diagnosis of fouling in heat exchangers. *Ind Eng Chem Res*. 2020;59:4602-4619.
34. Coletti F, Macchietto SA. A dynamic, distributed model of shell-and-tube heat exchangers undergoing crude oil fouling. *Ind Eng Chem Res*. 2011;50:4515-4533.
35. Caputo AC, Pelagagge PM, Salini P. Manufacturing cost model for heat exchangers optimization. *Appl Therm Eng*. 2016;94:513-533.
36. Saunders EAD. *Heat Exchangers: Selection, Design and Construction*. John Wiley & Sons; 1988.
37. Taborek J. Input data and recommended practices. In: Hewitt GF, ed. *Heat Exchanger Design Handbook*. . Begell House; 2008.
38. Incropera FPD, Witt DP. *Fundamentals of Heat and Mass Transfer*. 6th ed. John Wiley & Sons; 2006.
39. Diaz-Bejarano E, Coletti F, Macchietto S. Crude oil fouling deposition, suppression, removal, and consolidation—and how to tell the difference. *Heat Transfer Eng*. 2017;38:681-693.
40. Ishiyama EM, Paterson WR, Wilson DI. Thermo-hydraulic channelling in parallel heat exchangers subject to fouling. *Chem Eng Sci*. 2008;63:3400-3410.
41. Polley GT, Wilson DI, Yeap BL, Pugh SJ. Evaluation of laboratory crude oil threshold fouling data for application to refinery pre-heat trains. *Appl Therm Eng*. 2002;22:777-788.
42. Loyola-Fuentes J, Smith R. Data reconciliation and gross error detection in crude oil pre-heat trains undergoing shell-side and tube-side fouling deposition. *Energy*. 2019;183:368-384.
43. Loyola-Fuentes J, Smith R. Classification and estimation of unmeasured process variables in crude oil pre-heat trains subject to fouling deposition. *Comput Chem Eng*. 2020;137:106779.
44. Diaz-Bejarano E, Coletti F, Macchietto S. Modeling and prediction of shell-side fouling in shell-and-tube heat exchangers. *Heat Transfer Eng*. 2019;40:846-861.
45. Nahes ALM, Martins NR, Bagajewicz MJ, Costa ALH. Computational study of the use of set trimming for the globally optimal design of gasketed-plate heat exchangers. *Ind Eng Chem Res*. 2021;60:1746-1755.
46. Ishiyama EM, Pugh SJ, Wilson DI. Incorporating deposit ageing into visualisation of crude oil preheat train fouling. *Process Integr Optim Sustain*. 2020;4:187-200.
47. Assis BCG, Lemos JC, Liporace FS, et al. Dynamic optimization of the flow rate distribution in heat exchanger networks for fouling mitigation. *Ind Eng Chem Res*. 2015;54:6497-6507.
48. Tian J, Wang Y, Feng X. Simultaneous optimization of flow velocity and cleaning schedule for mitigating fouling in refinery heat exchanger networks. *Energy*. 2016;109:1118-1129.

SUPPORTING INFORMATION

Additional supporting information may be found in the online version of the article at the publisher's website.

How to cite this article: Lemos JC, Costa ALH, Bagajewicz MJ. Design of shell and tube heat exchangers considering the interaction of fouling and hydraulics. *AIChE J*. 2022;68(5): e17586. doi:10.1002/aic.17586

15475905, 2022, 5, Downloaded from https://aiche.onlinelibrary.wiley.com/doi/10.1002/aic.17586 by University Of Oklahoma, Wiley Online Library on [04/11/2023]. See the Terms and Conditions (https://onlinelibrary.wiley.com/terms-and-conditions) on Wiley Online Library for rules of use; OA articles are governed by the applicable Creative Commons License